Theoretical study of in-plane response of magnetic field sensor to magnetic beads in an in-plane homogeneous field

Damsgaard, Christian Danvad; Hansen, Mikkel Fougt

Published in:
Journal of Applied Physics

Link to article, DOI:
10.1063/1.2890754

Publication date:
2008

Document Version
Publisher's PDF, also known as Version of record

Theoretical study of in-plane response of magnetic field sensor to magnetic beads in an in-plane homogeneous field

Christian Danvad Damsgaard and Mikkel Fougt Hansen[a)]
Department of Micro- and Nanotechnology, Technical University of Denmark, DTU Nanotech, Building 345 East, DK-2800 Kongens Lyngby, Denmark

(Received 24 August 2007; accepted 3 January 2008; published online 25 March 2008)

We present a systematic theoretical study of the average in-plane magnetic field on square and rectangular magnetic field sensors from a single magnetic bead and a monolayer of magnetic beads magnetized by an in-plane externally applied homogeneous magnetic field. General theoretical expressions are derived such that the sensor response and its dependence on the sensor size, spacer layer thickness, bead diameter, and bead susceptibility can easily be evaluated. The average magnetic field from a single bead close to the sensor shows a strong dependence on the position of the bead and a change of sign when the bead passes the edge of the sensor in the direction of the applied field. Analytical approximations are derived for the average field from a homogeneous monolayer of beads for beads much smaller than the sensor dimension and for a bead size chosen to minimize the position sensitivity of the sensor response. We discuss implications for the sensor design and give general guidelines for optimum choices of sensor dimension, spacer layer thickness, and bead diameter, as well as simple expressions for the average magnetic field from the beads. The usage of the general guidelines is exemplified in the design considerations for a sensor, which is fully covered by 100 beads and has a spacer layer thickness of 100 nm. © *2008 American Institute of Physics*. [DOI: 10.1063/1.2890754]

I. INTRODUCTION

Magnetic biosensors combine a sensitive magnetic field sensor with a bioassay that ensures specific binding of micrometer-sized or submicrometer-sized magnetic beads to the sensor surface when the target biological substance, for example virus, proteins, or DNA, is present in the sample. Due to the direct electrical readout, the potential portability, and potentially very high sensitivity, magnetic biosensors have received considerable attention in the literature (for reviews, see Refs. 1–4). A wide spectrum of sensor principles has been suggested ranging from giant magnetoresistance multilayer stacks,[5–7] spin valves,[1–3,8–12] magnetic tunnel junctions,[13] ordinary Hall sensors,[14] and planar Hall effect sensors.[15,16] Most of these, and in particular the spin valves, magnetic tunnel junctions, and planar Hall effect sensors, rely on detection of the component of the magnetic field from the beads in the plane of the sensor.

The beads generally show superparamagnetic properties and only have a nonzero magnetic moment when they are magnetized by either an external magnetic field or by the magnetic field from the sensing current passed through the sensor. Their presence is detected as a change of the field experienced by the sensor. An ideal magnetic biosensor has an output electrical signal, which is proportional to the amount or concentration of the biological target. Hence, the reliability of the magnetic biosensor depends both on the specificity of the biological assay and the relation between the electrical response and the bead coverage of the sensor. Moreover, one must ensure that the result is statistically significant either by having many parallel sensors or by increasing the sensor area. Only a few examples of calculations of the sensor response to a specific bead coverage exist.[3,9–11] These are mostly based on particular arrangements of either a single bead or an array of beads, and do generally not systematically investigate the variation in the average magnetic field with the bead position, the effect of beads placed outside the sensor area, and the influence of sensor and bead parameters.

Here, we present a systematic general study of the response of a linear sensor with a square or a rectangular geometry to a single magnetic bead and a monolayer of magnetic beads in an in-plane externally applied homogeneous magnetic field as a function of the sensor dimension, the spacer layer thickness, the bead diameter, the bead susceptibility, and the position of the beads. The square geometry is relevant for our own work on planar Hall effect biosensors, and the rectangular geometry is relevant for most spin-valve sensors. We show and quantify that, for most geometries employed in magnetic biosensors, the sensor response depends strongly on the position of the magnetic bead and that it changes sign for beads just outside the sensor area. Guidelines are extracted from the general analysis that should be considered in the work on magnetic biosensors.

II. THEORY

A. General assumptions and considerations

We assume that the response of the sensor is linear, and that the sensor responds to the local magnetic field acting on the sensor, i.e., that different regions of the sensor act independently of each other. These assumptions ensure that the

[a)]Electronic mail: mfh@mic.dtu.dk.

sensor response is given by the sensitivity times the average magnetic field acting on the sensor. The sensor will therefore respond to

$$\langle \mathbf{H} \rangle = \mathbf{H}_{\text{ext}} + \langle \mathbf{H}_b \rangle, \tag{1}$$

where $\mathbf{H}_{\text{ext}}$ is the field acting on the sensor in the absence of beads, and $\langle \mathbf{H}_b \rangle$ is the average magnetic field due to the presence of magnetic beads. This field is in general for a bead number density $n(\mathbf{r}_0)$ given as

$$\langle \mathbf{H}_b \rangle = \frac{1}{A} \int_V n(\mathbf{r}_0) \int_A \mathbf{H}_b(\mathbf{r}, \mathbf{r}_0) d\mathbf{r} d\mathbf{r}_0, \tag{2}$$

where A is the sensor area and $\mathbf{H}_b(\mathbf{r}, \mathbf{r}_0)$ is the magnetic field strength observed in position $\mathbf{r}=(x,y,z)$ from a single magnetic bead at the position $\mathbf{r}_0=(x_0,y_0,z_0)$.

We assume that the magnetic beads are magnetized by a homogeneous external magnetic field $\mathbf{H}_{\text{ext}}$. Moreover, we assume that the beads are spherical and uniformly magnetized with a superparamagnetic response such that the field from a bead can be represented by the dipole field,

$$\mathbf{H}_b(\mathbf{r}, \mathbf{r}_0) = \frac{\chi R^3}{3} \left[\frac{3[\mathbf{H}_{\text{ext}} \cdot (\mathbf{r} - \mathbf{r}_0)](\mathbf{r} - \mathbf{r}_0)}{|\mathbf{r} - \mathbf{r}_0|^5} - \frac{\mathbf{H}_{\text{ext}}}{|\mathbf{r} - \mathbf{r}_0|^3} \right], \tag{3}$$

where R is the radius and χ is the constant effective magnetic susceptibility of a bead. This expression is valid when the magnetic interactions between the magnetic beads are negligible, that is, when the dipole field from neighboring beads is much smaller than $\mathbf{H}_{\text{ext}}$. Using the dipole field from Eq. (3), this results in the criterion

$$\frac{\chi R^3}{3 r_{bb}^3} \ll 1, \tag{4}$$

where r_{bb} is the center-to-center distance of two beads. Due to demagnetization effects, the effective magnetic susceptibility of the beads fulfills $\chi \leq 3$ and for many commercial beads $\chi \lesssim 1$. Hence, the criterion reduces to $r_{bb}^3 \gg R^3$. As $r_{bb} \geq 2R$, we have $r_{bb}^3 \geq 8R^3$ and the criterion will be fulfilled in most cases. Therefore, bead-bead interactions may play a non-negligible role for close-packed beads, but for less densely packed bead configurations they are unimportant. Below, we will consider the beads as noninteracting.

In addition to the externally applied homogeneous magnetic field, the sensor itself may give rise to a magnetostatic field from the magnetic layers in the structure, and the sensing current passed through the sensor gives rise to a self-field.[17] To simplify the treatment below, we will assume that the magnetostatic field is negligible compared to $\mathbf{H}_{\text{ext}}$. The self-field may be significant but can be reduced by using a lower bias current. Note that the self-field does not affect ordinary lock-in measurements carried out by modulating either the sensor current or the applied magnetic field if a sufficiently high time constant is used. Thus, the results below are valid for lock-in measurements or for a negligible self-field.

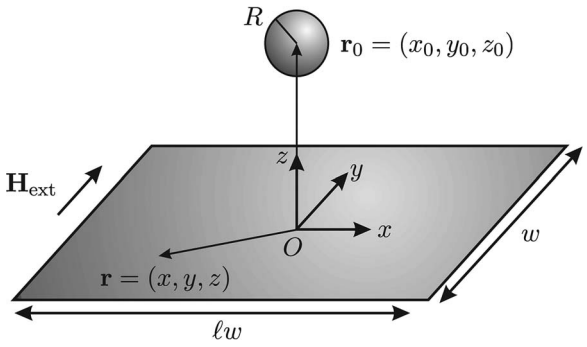

FIG. 1. Sketch of the system of interest: The external magnetic field is chosen to be fixed in the y-direction. The sensor is in the xy plane and has side lengths ℓw and w in the x- and y-directions, respectively. The origin (O) of the coordinate system is in the center of the sensor.

B. Geometry and normalized variables

We consider a sensor with side lengths ℓw and w in the x- and y-directions, respectively, and define a coordinate system with its origin in the center of the sensor as sketched in Fig. 1. The external magnetic field is applied along the y-direction, $\mathbf{H}_{\text{ext}}=H_{\text{ext}}\,\hat{\mathbf{y}}$. We will restrict ourselves to only consider the effect of the field from the beads in the y-direction as the components of the bead field in the x- and z-directions will typically have a negligible influence on the sensor response for the considered sensor types.

It is convenient to introduce the dimensionless geometric variables $\tilde{\mathbf{r}}=2\mathbf{r}/w$, $\tilde{\mathbf{r}}_0=2\mathbf{r}_0/w$, and $\tilde{R}=2R/w$. Moreover, we also introduce the normalized magnetic field,

$$\tilde{H} = \frac{H}{\frac{1}{3}\chi H_{\text{ext}} \tilde{R}^3}. \tag{5}$$

For a single bead with its center at $\tilde{\mathbf{r}}=(\tilde{x}_0,\tilde{y}_0,\tilde{z}_0)$, the normalized y-component of the dipole field at the sensor, $\tilde{\mathbf{r}}=(\tilde{x},\tilde{y},0)$, is

$$\tilde{H}_{by}(\tilde{x},\tilde{y},\tilde{\mathbf{r}}_0) = \frac{2(\tilde{y}-\tilde{y}_0)^2 - (\tilde{x}-\tilde{x}_0)^2 - \tilde{z}_0^2}{[(\tilde{x}-\tilde{x}_0)^2 + (\tilde{y}-\tilde{y}_0)^2 + \tilde{z}_0^2]^{5/2}}. \tag{6}$$

The average field from a single bead is then

$$\langle \tilde{H}_{by}(\tilde{\mathbf{r}}_0) \rangle = \frac{1}{4\ell} \int_{-1}^{1} \int_{-\ell}^{\ell} \tilde{H}_{by}(\tilde{x},\tilde{y},\tilde{\mathbf{r}}_0) d\tilde{x} d\tilde{y}, \tag{7}$$

and Eq. (2) assumes the form

$$\langle \tilde{H}_{by} \rangle = \int_{\tilde{V}} \tilde{n}(\tilde{\mathbf{r}}_0) \langle \tilde{H}_{by}(\tilde{\mathbf{r}}_0) \rangle d\tilde{\mathbf{r}}_0, \tag{8}$$

where we have defined $\tilde{n}(\tilde{\mathbf{r}}_0) \equiv (w/2)^3 n(\mathbf{r}_0)$. Below, we use the notation that an averaging has been carried out over space variables (e.g., $\tilde{\mathbf{r}}_0$) when these are not explicitly mentioned.

C. Calculation scheme for bead monolayers

The average field acting on the sensor from one or several beads placed at positions $\tilde{\mathbf{r}}_i$ is described using Eq. (8) with $\tilde{n}(\tilde{\mathbf{r}}) = \Sigma_i \delta(\tilde{\mathbf{r}} - \tilde{\mathbf{r}}_i)$. The evaluation of this sum becomes unfeasible when many beads are involved, and in this case it

is relevant to use a continuous representation of the bead distribution. A continuous representation is valid when a substantial number of beads are present and when they are small compared to the sensor dimension, i.e., when $\tilde{R} \ll 1$. If the beads are large or only a few beads are present, such a representation will only be valid for the statistical average over many sensors. A special case occurs when the bead distribution is homogeneous, i.e., when any structure in the distribution has a length scale much smaller than the sensor dimension. In this case the average field from the beads can be calculated from a constant distribution $\tilde{n}(\tilde{\mathbf{r}})$, which is nonzero where the beads are placed. For a single layer of beads, we write

$$\tilde{n}(\tilde{x},\tilde{y},\tilde{z}) = \frac{\delta(\tilde{z}-\tilde{z}_0)}{\alpha \tilde{R}^2}, \tag{9}$$

where αR^2 is the area taken up by a bead in the packed structure. For example, for a hexagonal close-packed (hcp) arrangement of beads, $\alpha_{\mathrm{hcp}} = 2\sqrt{3}$. Equation (8) can conveniently be evaluated numerically. A packing density representing another homogeneous distribution of magnetic beads can be introduced by scaling the calculated average magnetic field with the ratio of the packing densities. This and the normalization of the variables makes the results of the calculations generally applicable.

Finally, it is useful to discuss consequences of a homogeneous bead layer, which is infinite in the sensor plane and for which $\tilde{R} \ll 1$. This layer can be approximated by a continuous plate of a magnetizable material. From Ampère's law, it is easily shown that the **H**-field is identical to the external magnetic field, and hence that $\mathbf{H}_b = 0$. Thus, an infinite bead monolayer in a homogeneous external magnetic field does not give rise to any sensor response. Dividing an infinite plane into an area inside the sensitive area on top of the sensor and outside this area, we obtain

$$\langle \mathbf{H}_b^{\mathrm{inside}} \rangle = -\langle \mathbf{H}_b^{\mathrm{outside}} \rangle, \tag{10}$$

where $\langle \mathbf{H}_b^{\mathrm{inside}} \rangle$ is the average magnetic field on the sensor region from a homogeneous layer of beads positioned inside the sensor region, and $\langle \mathbf{H}_b^{\mathrm{outside}} \rangle$ is the average magnetic field on the sensor region from a homogeneous layer of beads positioned outside the sensor region. This relation will be useful later for estimating the response of a sensor with shielding layers to a monolayer of beads, as one only needs to integrate over beads on the sensitive area of the sensor.

III. RESULTS

Below, we present calculations of the normalized average magnetic field $\langle \tilde{H}_{by} \rangle$, first as a function of the normalized position $(\tilde{x}_0, \tilde{y}_0, \tilde{z}_0)$ of a single magnetic bead, and then for monolayers of magnetic beads.

A. Single bead results

An analytical expression for the average magnetic field from beads positioned at $(\tilde{x}_0, 0, \tilde{z}_0)$ is accessible but rather unhandy. For a bead positioned over the sensor center, $\tilde{\mathbf{r}}_0 = (0,0,\tilde{z}_0)$, the analytical expression is

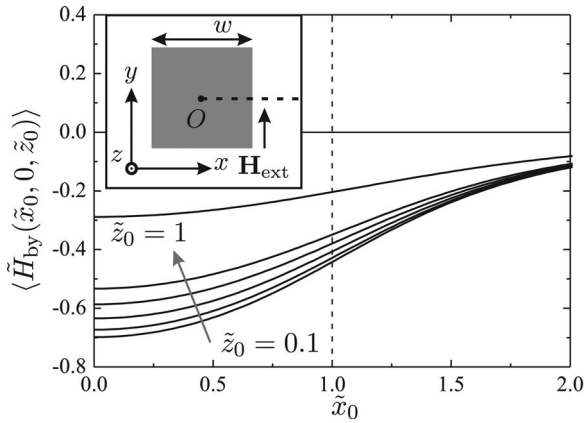

FIG. 2. Normalized average magnetic field in the y-direction from a single bead at the position $(\tilde{x}_0, 0, \tilde{z}_0)$ of a square sensor ($\ell = 1$) as a function of $\tilde{x}_0$ for $\tilde{z}_0 = 0.1$, 0.2, 0.3, 0.4, 0.5, 1 (increasing values indicated by arrow). The sensor edge is at $\tilde{x}_0 = 1$. The inset shows the sensor geometry; the investigated values of $\tilde{x}_0$ are indicated by the dashed line.

$$\langle \tilde{H}_{by}(0,0,\tilde{z}_0) \rangle = -\frac{1}{(1+\tilde{z}_0^2)(1+\ell^2+\tilde{z}_0^2)^{1/2}}. \tag{11}$$

Below, we present results for square sensors ($\ell = 1$). For rectangular sensors with $\ell > 1$, the general results and conclusions will be the same, but some of the exact numbers will be slightly larger due to the reduced effect of the edges at $|\tilde{x}| = \ell$.

Figure 2 shows the normalized average magnetic field from a magnetic bead positioned in the $\tilde{x}\tilde{z}$ plane of a square sensor calculated using Eq. (7). The function is symmetric around $\tilde{x}_0 = 0$. The field is negative as expected for a dipole, and attains its minimum in the center of the sensor. The minimum value is given by Eq. (11), which for small values of $\tilde{z}_0$ and $\ell = 1$ yields $\langle \tilde{H}_{by}(0,0,\tilde{z}_0) \rangle \approx -(1/\sqrt{2})(1 - \frac{5}{4}\tilde{z}_0^2)$. Thus, when the beads are small compared to the sensor dimension and placed in the $\tilde{x}\tilde{z}$ plane, the average magnetic field depends only weakly on the separation from the sensor. For increasing $\tilde{x}$ the magnitude of the magnetic field gradually drops towards zero.

Figure 3 shows the normalized average magnetic field from a magnetic bead positioned in the $\tilde{y}\tilde{z}$ plane calculated using Eq. (7). The function is symmetric around $\tilde{y}_0 = 0$. In this case, the dependency on the position is much stronger, and for low $\tilde{z}_0$ values the average magnetic field from the bead drops to large negative values when the bead approaches the sensor edge ($\tilde{y}_0 < 1$) and attains correspondingly large positive values when the bead is just outside the sensor edge ($\tilde{y}_0 > 1$). This can be explained as follows: The dipole field from the bead close to the sensor surface has large positive contributions at the sensor near its magnetic north and south poles and a large negative contribution just below the bead (see the lower inset of Fig. 3). When the bead is near the center of the sensor these two contributions almost cancel and result in a small negative average magnetic field. When the bead approaches the sensor edge along the external magnetic field (positive y-direction), the positive contribution near the magnetic north pole of the bead is now outside the sensor and the strong negative contribution just below the bead dominates, giving rise to a negative peak in

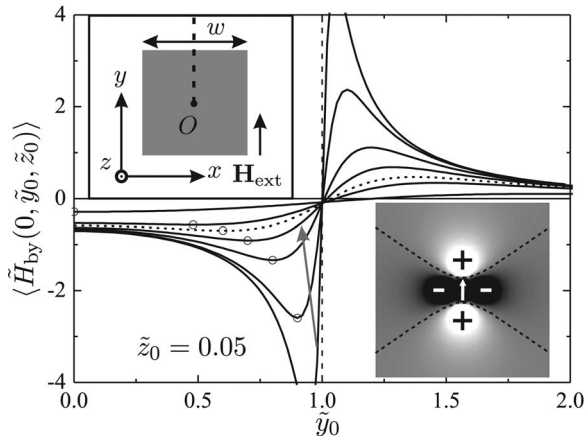

FIG. 3. Normalized average magnetic field in the y-direction from a single bead at the position $(0,\tilde{y}_0,\tilde{z}_0)$ on a square sensor ($\ell=1$) as a function of $\tilde{y}_0$ for $\tilde{z}_0$=0.05, 0.1, 0.2, 0.3, 0.4 (dashed), 0.5, 1 (increasing values indicated by arrow). The sensor edge is at $\tilde{y}_0$=1. The circles on the curves indicate $(\tilde{y}_{\min},\langle \tilde{H}_{\text{by}}(0,\tilde{y}_{\min},\tilde{z}_0)\rangle)$. The top inset shows the sensor geometry; the investigated values of $\tilde{y}_0$ are indicated by the dashed line. The bottom inset shows a gray-scale plot of the y-component of the dipole field just below a bead placed in the center magnetized as indicated by the arrow. In the inset, the dashed lines indicates the positions where the dipole field changes sign. The y-component of the dipole field is positive in the white regions and negative in the black regions.

the average magnetic field. When the bead is outside the sensor, the negative contribution is reduced and the positive contribution near the magnetic south pole of the bead dominates, giving rise to a positive peak of similar magnitude in the average magnetic field.

These peaks of opposite sign in the average magnetic field have a crucial influence on the average magnetic field affecting the sensor, and will therefore be investigated further below. Let the $\tilde{y}$ value corresponding to the position of the negative peak of $\langle \tilde{H}_{by}(0,\tilde{y},\tilde{z}_0)\rangle$ in the $\tilde{y}\tilde{z}$ plane be denoted $\tilde{y}_{\min}$. Figure 4 shows $-\langle \tilde{H}_{by}(0,\tilde{y}_{\min},\tilde{z}_0)\rangle$ and $\tilde{y}_{\min}$ as a function of $\tilde{z}_0$.

When $\tilde{z}_0 \gtrsim 0.4$, it is seen from Fig. 4 that the negative peak diminishes, the value of $\tilde{y}_{\min}$ approaches zero, and the minimum value of the average magnetic field approaches

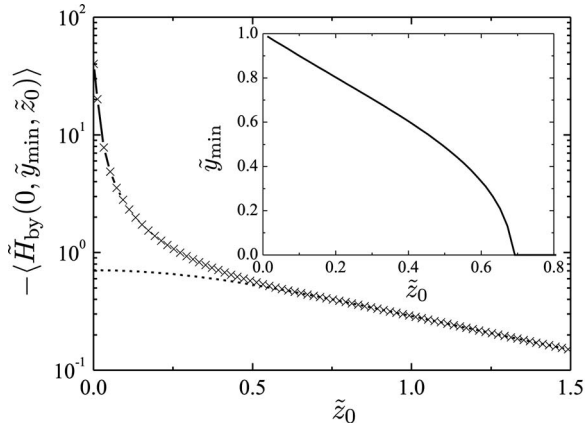

FIG. 4. Minimum average magnetic field as a function of $\tilde{z}_0$ for a square sensor. The dashed line corresponds to the average magnetic field from a bead position above the center of the sensor [Eq. (11)]. The inset shows the position of the minimum as a function of $\tilde{z}_0$.

that from a bead placed at the center of the sensor [Eq. (11)]. Upon further increase of $\tilde{z}_0$ beyond 0.5, Fig. 3 clearly shows a reduction of the sensitivity of the average magnetic field to beads placed close to the edge at $\tilde{y}_0$=1.

For $\tilde{z}_0 \lesssim 0.4$ the peak becomes clearly distinguishable, and it becomes meaningful to divide the sensor into an edge region of width $\approx 2(1-\tilde{y}_{\min})$ with an enhanced average sensitivity and a central region with a sensitivity corresponding to a bead placed in the center. An analysis of the data in Fig. 4 (not shown) reveals that the normalized average magnetic field for beads at $(0,\tilde{y}_{\min},\tilde{z}_0)$ in this region is proportional to $(\tilde{z}_0)^{-1}$.

B. Bead monolayer results

In this section, we calculate the average magnetic field from a monolayer with a packing constant α of beads on top of the sensitive region of the sensor only. The average magnetic field can be rewritten using Eq. (8) and the variable definitions as

$$\langle H_{by}(\tilde{z}_0)\rangle = -\frac{\chi H_{\text{ext}}\tilde{R}}{3\alpha} I_\ell(\tilde{z}_0), \tag{12}$$

with

$$I_\ell(\tilde{z}_0) \equiv -\frac{1}{4\ell}\int_{-1}^{1}\int_{-\ell}^{\ell}\int_{-1}^{1}\int_{-\ell}^{\ell} \tilde{H}_{by}[\tilde{x},\tilde{y},(\tilde{x}_0,\tilde{y}_0,\tilde{z}_0)] \times d\tilde{x}d\tilde{y}d\tilde{x}_0d\tilde{y}_0. \tag{13}$$

This integral represents an averaging of the signal from a bead as a function of its position over the sensor times the normalized area, 4ℓ, of the sensor.

First, we notice that when the beads are far from the sensor compared to the sensor dimensions, the magnetic field from a bead placed anywhere on the sensor area can be approximated by $\tilde{H}_{by} \approx -(\tilde{z}_0)^{-3}$ [cf. Eq. (6)]. In this limit, the integrals in Eq. (13) can easily be evaluated and yield $I_\ell(\tilde{z}_0) \approx 4\ell \times (\tilde{z}_0)^{-3}$. Thus, $I_\ell(\tilde{z}_0)$ shows the expected dipole-like decay with a proportionality factor given by the normalized area 4ℓ of the bead layer.

We first present the results for a square sensor ($\ell=1$), where edge effects are important in both the x- and y-directions. Subsequently, we present results for rectangular sensors with aspect ratios ℓ so large that the effects of the edges at $|\tilde{x}|=\ell$ do not significantly overlap.

1. Approximate expressions for square sensors ($\ell=1$)

Figure 5 shows values of $I_1(\tilde{z}_0)$ as a function of $\tilde{z}_0$. Two distinct regimes are found in the graph at low and high values of $\tilde{z}_0$, respectively, and fits to simple approximations are indicated. For $\tilde{z}_0 > 8.9$ and $\tilde{z}_0 > 6.3$ it is observed that the response is described by $I_1(\tilde{z}_0)=4\times(\tilde{z}_0)^{-3}$ within 5 and 10%, respectively. For $\tilde{z}_0 \lesssim 0.25$ and $\tilde{z}_0 \lesssim 0.35$ the response is described by

$$I_1(\tilde{z}_0) = -4.525 \times \log(\tilde{z}_0), \tag{14}$$

within 5 and 10%, respectively. In this regime the observed logarithmic divergence is a result of a balance between the contributions from beads near the edge at $|\tilde{y}_0|=1$ and those

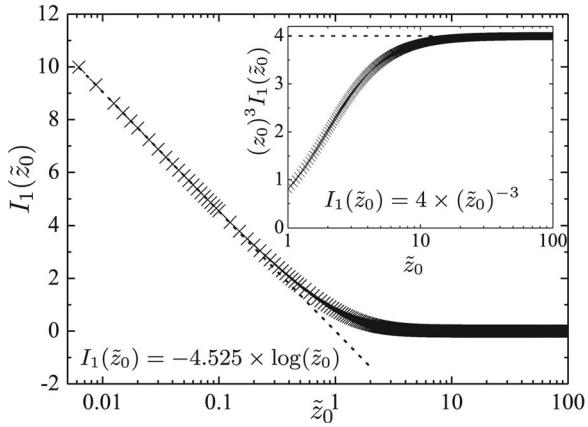

FIG. 5. Values of $I_1(\tilde{z}_0)=-\langle H_{by}(\tilde{z}_0)\rangle/(\chi H_{ext}\tilde{R}/3\alpha)$ calculated for a square sensor ($\ell=1$) as a function of $\tilde{z}_0$. The inset shows $(\tilde{z}_0)^3 I_1(\tilde{z}_0)$ for large values of $\tilde{z}_0$. The dashed lines are the indicated simple analytical approximations.

near the center of the sensor. The maximum contribution from the former scales as $\tilde{z}_0^{-1}$, whereas the contribution from the latter is essentially constant [cf. Fig. 4 and Eq. (11)].

2. Approximate expressions for rectangular sensors ($\ell > 1$)

For rectangular sensors the general behavior is the same as for the square sensors. In this section, we will therefore focus on estimating $I_\ell(\tilde{z}_0)$ at values of $\tilde{z}_0 < 1$, which are the relevant ones for most experimental work.

When the sensor aspect ratio ℓ is sufficiently large and $\tilde{z}_0$ is sufficiently small, the influence of the edges at $|\tilde{x}|=\ell$ is reduced and the sensor response becomes independent of $\tilde{x}_0$ in the central region of the sensor.

We choose to write

$$I_\ell(\tilde{z}_0) = I_{\text{center}}(\tilde{z}_0) - \ell^{-1} I_{\text{edge}}(\tilde{z}_0), \tag{15}$$

where $I_{\text{center}}(\tilde{z}_0)$ is the response when the effect of the edges at $|\tilde{x}|=\ell$ is neglected and $I_{\text{edge}}(\tilde{z}_0)$ represents the reduction of the response near the edges at $|\tilde{x}|=\ell$. The factor of ℓ^{-1} accounts for the relative influence of the edges at $|\tilde{x}|=\ell$. Figure 6(a) shows a log-lin plot of $I_{\text{center}}(\tilde{z}_0)$ calculated by using Eq. (13) for a sensor long enough to make edge effects unimportant as a function of $\tilde{z}_0$. The dependence on $\tilde{z}_0$ is clearly logarithmic and is found to be described by

$$I_{\text{center}}(\tilde{z}_0) = 1.410 - 4.589 \times \log(\tilde{z}_0), \tag{16}$$

within 5% for $\tilde{z}_0 < 0.73$ and within 10% for $\tilde{z}_0 < 0.92$. Figure 6(b) shows a lin-log plot of values of $I_{\text{edge}}(\tilde{z}_0)$ calculated by solving Eq. (15) for $I_{\text{edge}}(\tilde{z}_0)$ for a sensor with $\ell=3$ as a function of $\tilde{z}_0$. The dependence on $\tilde{z}_0$ is clearly exponential and is found to be described by

$$I_{\text{edge}}(\tilde{z}_0) = 1.829 \times 10^{-0.232 \times \tilde{z}_0}, \tag{17}$$

within 0.4% for $\tilde{z}_0 < 1$. These expressions make it possible to find $I_\ell(\tilde{z}_0)$ for any $\ell > 1$ as a function of small values of $\tilde{z}_0$. It is stressed that this description is only accurate when the effects of the edges at $|\tilde{x}|=\ell$ do not overlap significantly, and that the extension of the edge effects increases with increasing $\tilde{z}_0$. For example, for $\ell=1$, the error made by using Eq. (15) is about 33% for $\tilde{z}_0=1$ but less than 5% for $\tilde{z}_0 < 0.05$. For $\ell=2$, the corresponding error at $\tilde{z}_0=1$ is about 3%. A general investigation for values of ℓ ranging between 2 and 50 and various values of $\tilde{z}_0 \leq 1$ shows that Eq. (15) with the above expressions approximates the quadruple integral in Eq. (13) within 3% for $\ell > 2$, and that the approximation is better for smaller values of $\tilde{z}_0$ and larger values of ℓ.

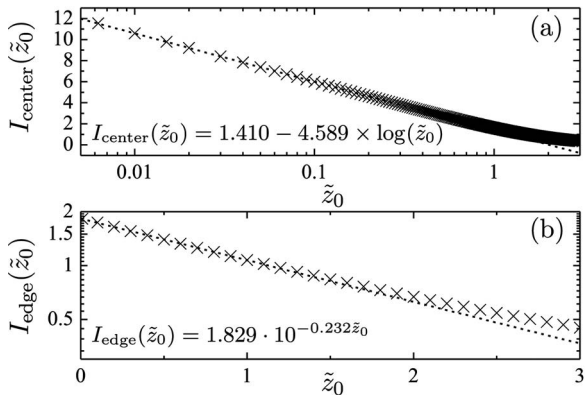

FIG. 6. Values of (a) $I_{\text{center}}(\tilde{z}_0)$ and (b) $I_{\text{edge}}(\tilde{z}_0)$ calculated as a function of $\tilde{z}_0$ as described in the text. The dotted lines and the written equations are analytical approximations valid for low values of $\tilde{z}_0$.

IV. DISCUSSION

In the discussion below, we consider beads placed on top of the sensor with $\tilde{z}_0=\tilde{R}+\tilde{t}$, where $\tilde{t}=2t/w$ is the normalized thickness of the spacer layer between the active sensor layer and the edge of the bead. This spacer layer consists of the surface coating and other inactive layers. We first discuss the response of single beads and then the response of a bead monolayer.

A. Single bead response

The detection of a single bead is best achieved when the sensor dimension is made comparable to or smaller than the bead dimension. For example, for $t=0$ a bead of diameter $2R=w$ placed on the center of a sensor gives rise to the average magnetic field $\langle H_{by}(0,0,\tilde{z}_0=1)\rangle=(6\sqrt{2+\ell^2})^{-1}\chi H_{ext}$. For the same bead, Fig. 3 indicates that edge effects in the y-direction are small when $\tilde{z}_0=2R/w \approx 0.3-0.5$ and become relevant when $\tilde{z}_0$ differs significantly from this range of values. For a square sensor we have performed a detailed analysis of the dependence of $\langle H_{by}(\tilde{x}_0,\tilde{y}_0,\tilde{z}_0)\rangle$ on the position $(\tilde{x}_0,\tilde{y}_0)$ of a bead on the sensor as function of $\tilde{z}_0$ and found that the ratio of the standard deviation of the obtained values to their mean value attained a minimum value of 27% for $\tilde{z}_0=0.36$. Thus, for $\tilde{z}_0=0.36$ the sensor response has the weakest dependency on the position of a bead on the sensor area. However, this ratio only varies little and assumes values below 28% for $0.30 < \tilde{z}_0 < 0.45$. For $\tilde{z}_0 \gtrsim 0.45$ the average field becomes significantly less sensitive to beads positioned just inside the $|\tilde{y}|=1$ edge of the sensor. For $\tilde{z}_0 \lesssim 0.3$ the average field becomes increasingly sensitive to beads positioned near $\pm\tilde{y}_{\min}$. Moreover, the average magnetic field changes sign when the bead passes the sensor edge and exhibits a similar positive peak just outside the sensor. Thus,

the field from a single bead can give rise to positive or negative average magnetic fields of similar magnitude depending on its position relative to the sensor. This may be an undesirable property of a sensor, and precautions must be taken to minimize this contribution.

B. Bead monolayer response

The average magnetic field from a bead monolayer on top of a sensor can be found by the use of Eq. (12) with $I_\ell(\tilde{z}_0)$ found from Fig. 5 or the approximation in Eq. (14) for low $\tilde{z}_0$ values for square sensors ($\ell=1$) or from Eqs. (15)–(17) for rectangular sensors ($\ell>1$). We first discuss the average field acting on the sensor when the beads are small compared to w, and then proceed to discuss when the spacer layer thickness and bead diameter are chosen to minimize the peaks in the sensitivity to the position of beads near the sensor edges at $|\vec{y}|=1$.

An important parameter is the number of beads N_ℓ that can fit onto a sensor in a given arrangement. This number is

$$N_\ell \approx \frac{\ell w^2}{\alpha R^2} \tag{18a}$$

$$= \frac{4\ell}{\alpha \tilde{z}_0^2}\left(\frac{R+t}{R}\right)^2 \tag{18b}$$

$$= \frac{\ell}{\alpha}\left(\frac{1}{2}\tilde{z}_0 - \frac{t}{w}\right)^{-2}, \tag{18c}$$

where we have used $2R=\tilde{z}_0 w-2t$ to get the last expressions. Note that these expressions are only valid for $\tilde{z}_0>2t/w$. For a hcp arrangement where $\alpha_{\mathrm{hcp}}=2\sqrt{3}$, we denote the number as $N_{\ell,\mathrm{hcp}}$. For the arguments in the discussion, it will be convenient to write Eq. (12) in the forms

$$-\frac{\langle H_{by}\rangle}{\frac{1}{3\alpha}\chi H_{\mathrm{ext}}} = I_\ell(\tilde{z}_0)\left[\frac{\tilde{z}_0 w-2t}{w}\right] \tag{19a}$$

$$= \tilde{z}_0 I_\ell(\tilde{z}_0)\frac{R}{R+t} \tag{19b}$$

$$= 2\ell^{1/2}\alpha^{-1/2} I_\ell(\tilde{z}_0) N_\ell^{-1/2}. \tag{19c}$$

From Eq. (19b) it is seen that the sensor response for a fixed $\tilde{z}_0$ value is independent of the bead size when $t \ll R$. Hence, t should be kept well below the bead radius to avoid a significant reduction of the average field. The maximum of the magnitude of the normalized average magnetic field coincides with that of $\tilde{z}_0 I_\ell(\tilde{z}_0)$. An investigation for square sensors using the results in Fig. 5 yields that $\tilde{z}_0 I_1(\tilde{z}_0)$ increases with increasing $\tilde{z}_0$ up to $\tilde{z}_0 \approx 0.6$, where it attains its maximum value of 0.870. Thus, for fixed values of all parameters except $\tilde{z}_0$ and $2R$, the average magnetic field grows with increasing bead diameter for $\tilde{z}_0<0.6$. For $t \ll R$, the maximum corresponds to a bead diameter of $2R=0.6w$ and a sensor coverage of three beads. A similar result is obtained for rectangular sensors. For such large bead diameters, the assumption of a homogeneous coverage is no longer fulfilled and one should sum single bead contributions.

TABLE I. Calculated parameters for a square sensor ($\ell=1$) and for the indicated values of $\tilde{z}_0$ and w. For each value of w the values in the three rows are from top to bottom: Bead diameter $2R=\tilde{z}_0 w-2t$ (μm) (top), number of beads in hcp arrangement $N_{1,\mathrm{hcp}} \approx w^2/2\sqrt{3}R^2$ (middle), normalized average magnetic field from monolayer $\langle H_{\mathrm{by}}\rangle/(\chi H_{\mathrm{ext}}/3\alpha)=(2R/w)I_1(\tilde{z}_0)$ (bottom). The value $t=100$ nm has been used in all calculations.

$\tilde{z}_0=$	0.0125	0.025	0.05	0.1	0.2	0.4
			0.05	0.3	0.8	1.8
$w=5$ μm	⋯	⋯	11 547	321	45	9
			0.059	0.273	0.521	0.744
		0.05	0.3	0.8	1.8	3.8
$w=10$ μm	⋯	46 188	1 283	180	36	8
		0.036	0.176	0.363	0.586	0.785
	0.05	0.3	0.8	1.8	3.8	7.8
$w=20$ μm	184 752	5 132	722	143	32	8
	0.022	0.109	0.235	0.409	0.619	0.806
	0.3	0.8	1.8	3.8	7.8	15.8
$w=40$ μm	20 528	2 887	570	128	30	7
	0.065	0.145	0.265	0.432	0.635	0.816

Equation (19c) shows that for a fixed value of $\tilde{z}_0$ and a given packing of the beads, the average field from a monolayer is inversely proportional to the square root of the number of beads that can fit onto the sensor. This again shows that the signal is larger from a sensor with space for only a few beads. It is also seen that for fixed N_ℓ, α, and $\tilde{z}_0$, a larger response can be obtained for larger values of ℓ. This reflects that the bead diameter becomes larger for constant N_ℓ and $\tilde{z}_0$ when ℓ increases.

Even for a square sensor, the average magnetic field from a bead monolayer has a complicated dependence on the bead diameter ($2R$), spacer layer thickness (t), $\tilde{z}_0$, and the sensor dimension (w). Only three of these four variables are independent. Table I shows the calculations of the bead diameter, the number of beads, and the normalized average magnetic field for a range of typical choices of $\tilde{z}_0$ and w. We have chosen these parameters as w defines the (relatively fixed) sensor geometry and $\tilde{z}_0$ determines whether edge effects are important. The calculations were carried out for a spacer layer thickness of $t=100$ nm. Using this table, it is easy to relate the average magnetic field from the monolayer to the bead size, the number of beads in a monolayer, and the sensor dimension.

1. Beads small compared to sensor dimension

Let us first consider the case of beads that are small compared to the sensor dimension, $\tilde{z}_0 \leq 0.1$ ($2R \leq 0.1w-2t$). In this case, a close-packed monolayer of magnetic beads on a square sensor contains more than 100 magnetic beads (Table I).

For a fixed value of $\tilde{z}_0$, Eq. (19a) and Table I show that the average magnetic field is significantly reduced when $2t$ becomes comparable to $\tilde{z}_0 w$. The reason for this is that the finite value of t reduces the bead size corresponding to the considered value of $\tilde{z}_0$.

For a fixed value of w, Table I shows that the average magnetic field depends strongly on the bead size and is par-

ticularly sensitive to the bead size for small sensor dimensions. Again, the explanation is that the smaller sensor dimension has a lower value of $\tilde{z}_0 w$ and thus enhances the negative effect of the spacer layer. For a square sensor with $w=10$ μm, for example, the average magnetic field is reduced by a factor of 2.1 when going down in bead diameter from 0.8 μm ($\tilde{z}_0=0.1$) to 0.3 μm ($\tilde{z}_0=0.05$). For $w=40$ μm, the reduction going from $\tilde{z}_0=0.1$ to $\tilde{z}_0=0.05$ is only a factor of 1.6.

For a fixed bead diameter, it is seen from Table I that the average magnetic field varies significantly with the sensor dimension. For $2R=0.8$ μm, for example, the normalized average magnetic field from a monolayer is reduced by a factor of 2.5 going from $w=10$ μm to $w=40$ μm. However, it should also be noted that the number of beads in a full monolayer increases by a factor of 16.0 from 180 to 2887.

The effect of a value of $\ell>1$ is to reduce the effect of the edges at $|\tilde{x}_0|=\ell$. For example, for $\tilde{z}_0=0.1$ and $\ell>2$ we have $I_1(0.1)\approx 4.53$ and $I_\ell(0.1)=6.00-1.74\ell^{-1}$. This shows that that for a square sensor and $\tilde{z}_0=0.1$ the edges at $|\tilde{x}_0|=1$ result in a reduction of the response due to a monolayer of beads by 26% compared to an infinitely long sensor. For $\tilde{z}_0=0.01$ the reduction is 15%. Thus, when the beads are small compared to w only little can be gained by increasing the sensor aspect ratio.

2. Bead size chosen to reduce edge effects at $|\tilde{y}_0|=1$

Different sensitivities to beads placed near the sensor edges at $|\tilde{y}|=1$ and the sensor center may be undesirable as the proportionality between the average magnetic field and the number of beads will clearly be affected. However, if a large number of beads are distributed homogeneously over the sensor area, the sensor response is still expected to be proportional to the bead coverage. As discussed in Sec. IV A, the edge effects are minimized when $\tilde{z}_0\approx 0.36$. This corresponds to a bead diameter of $2R=0.36w-2t$. Equation (19a) then yields $\langle H_{\mathrm{by}}\rangle=-(\chi H_{\mathrm{ext}}/3\alpha)[0.36-(2t/w)]I_\ell(0.36)$. For a square sensor we have $I_1(0.36)=2.24$, and for a rectangular sensor with $\ell\geq 2$ we have $I_\ell(0.36)=3.45-1.51\ell^{-1}$. This shows that that for a square sensor and $\tilde{z}_0=0.36$ the edges at $|\tilde{x}_0|=1$ result in a reduction of the response due to a monolayer of beads by 35% compared to an infinitely long sensor. The corresponding number of beads that can fit onto the sensor in a close-packed layer is given by Eq. (18c) and is $N_{\ell,\mathrm{hcp}}\approx \ell(2\sqrt{3})^{-1}(0.18-t/w)^{-2}$. If $t\ll w$, $N_{1,\mathrm{hcp}}\approx 9$, which is consistent with Table I. Note, however, that if the beads are large or only a few beads are present, the calculations only describe the statistical average over an ensemble of sensors with randomly placed beads, and single experimental observations will be better described by summing over the observed positions of the individual beads. If t is no longer much smaller than w, the bead size corresponding to $\tilde{z}_0=0.36$ is reduced and more beads can fit onto the sensor. This will be discussed further in Sec. IV C.

C. Implications for sensor design

We first emphasize the importance of reducing the number of beads placed outside the active sensor area, in particular along the direction of the applied field, to an absolute minimum. These beads contribute to the average field with a positive sign and thus reduce the response to beads placed on the sensor. This can be carried out (1) by designing a highly specific assay that ensures that beads are only coupled to the active area of the sensor, or (2) by using a physical shielding of the surroundings of the sensor area that ensures that beads outside the sensor area are kept at a distance large enough to make their contributions to the average magnetic field negligible. The required thickness T of such a shielding layer can be obtained as follows: Eq. (10) yields that the average field from a monolayer of beads outside the active area equals minus the average field from a monolayer of beads placed inside the active area. Note that this estimate is based on results for an infinite layer of beads and therefore will overestimate the influence of the beads outside the sensor compared to a layer of beads with finite dimensions. The shielding layer results in that the beads outside the active area are being placed at $\tilde{z}_0'>\tilde{z}_0$. The reduction of the average magnetic field from beads outside the active area relative to that from the beads inside the active area can then be estimated as $I_\ell(\tilde{z}_0')/I_\ell(\tilde{z}_0)$ [cf. Eq. (19c)].

For example, if $\tilde{z}_0=0.1$ for beads placed on a square sensor, and the average field from a monolayer of beads outside the sensor area should be a factor of 5 lower than that from beads inside the sensor area, we estimate from Fig. 5 that $\tilde{z}_0'\approx 0.9$ and that the shielding layer should have a total thickness of $T=z_0'-R=\frac{1}{2}\tilde{z}_0' w-R=0.45w-R$.

As we have seen, the choices of sensor and bead dimensions also strongly influence the response of the sensor; we found that the largest signal is obtained for beads with dimensions approaching the sensor size. In the literature, there has been a drive toward reducing the sensor dimension to be comparable to the bead dimension with the goal of detecting single magnetic beads.[7,8,11,14] Such sensors, although highly sensitive, have a limited applicability as reliable magnetic biosensors because of their sensitivity to the position of a single or very few beads. Unless many of those sensors are used in parallel, it is statistically very difficult to distinguish a real signal from that due to the inevitable background of unspecifically bound magnetic beads. The sensor and bead dimensions should be chosen as a result of a compromise between maximizing the average magnetic field from a monolayer of beads and being able to assess the background contribution from unspecifically bound beads with statistical significance. The best compromise between sensitivity and specificity depends on the background level and the sensor characteristics. The results of the present work can be used to make sensible choices of parameters based on the assay specificity and sensor signal-to-noise ratio.

We now consider a sensor with a given spacer layer thickness $t>0$ and discuss how to calculate and optimize values of the sensor dimension (w), the bead diameter ($2R$), the normalized distance from the bead center to the sensor surface ($\tilde{z}_0$), the maximum number of beads that can fit onto the sensor area (N_ℓ), and the average magnetic field. Below, we consider four different cases where one or more of these parameters are given and the rest are to be calculated and, if possible, optimized:

(1) Let ℓ, w, and $2R$ be given. Then, N_ℓ is given by Eq. (18a), $\tilde{z}_0=(2R+2t)/w$, and the average magnetic field is given by Eq. (19a).
(2) Let ℓ, $\tilde{z}_0$, and $2R$ be given. Then, $w=(2R+2t)/\tilde{z}_0$, N_ℓ is given by Eq. (18b), and the average magnetic field is given by Eq. (19b).
(3) Let ℓ, $\tilde{z}_0$, and $N_\ell > \ell\alpha^{-1}(\frac{1}{2}\tilde{z}_0)^{-2}$ be given. Then, w is found by solving Eq. (18c) as $w=t\left[\frac{1}{2}\tilde{z}_0-(\alpha\ell^{-1}N_\ell)^{-1/2}\right]^{-1}$, the bead diameter is $2R=\tilde{z}_0 w-2t$, and the average magnetic field is given by Eq. (19c).
(4) Let ℓ and N_ℓ be given. To maximize the average magnetic field, $I_\ell(\tilde{z}_0)$ should be maximized [Eq. (19c)] and hence $\tilde{z}_0$ should be minimized (Figs. 5 and 6). Using Eq. (18b), we write $\tilde{z}_0=2\ell^{1/2}(\alpha N_\ell)^{-1/2}(R+t)/R$. Thus, the minimum value $\tilde{z}_0=2\ell^{1/2}(\alpha N_\ell)^{-1/2}$ is obtained when $R\gg t$. For any choice of the bead diameter fulfilling $2R\gg 2t$, the corresponding w is found by solving Eq. (18a) and the average magnetic field is found from Eq. (19c) using the approximations for low-$\tilde{z}_0$ values described in Sec. III B.

In case (4), the increase in average magnetic field is due to the strongly increasing edge sensitivity for decreasing values of $\tilde{z}_0$ (cf. Figs. 3 and 4). Note that this observation is not in conflict with the discussion after Eq. (19b), where the bead number was free and the maximum result for square sensors was obtained for $\tilde{z}_0\approx 0.6$. Also note that a very high sensitivity to the bead position is not desired as it can make the average field from similar bead coverages fluctuate.

Let us consider two numerical examples for a square sensor where we require that 100 beads fit onto the sensor in a hcp arrangement.

First, we choose $\tilde{z}_0=0.36$ to ensure that edge effects are minimized and hence that the average magnetic field is proportional to the number of beads on the sensor. We term this operation mode "minimum position dependency." Using case (3) from above, we find that $w=7.92t$, $2R=0.851t$, and $\langle H_{by}\rangle=-0.0232\chi H_{\text{ext}}$. If t is small, the sensor and bead sizes may be unfeasible and then t should be increased by introducing an extra spacer layer. For example, if $w=5$ μm, we find that a spacer layer of thickness $t\approx 630$ nm and a bead diameter of $2R\approx 540$ nm should be used. For comparison, $t=100$ nm and the same values of w and $2R$ yield $\tilde{z}_0=0.148$ and a magnitude of the average field, which is a factor of $I_1(0.148)/I_1(0.36)=1.7$ times that obtained for $\tilde{z}_0=0.36$.

Second, we want to maximize the average magnetic field for our fixed choice of $N_1=100$ using case (4) from above. We term this operation mode "maximum response." For example, if $t=100$ nm and we choose $2R=2$ μm, we find $w=(2\sqrt{3}N)^{1/2}R=18.6$ μm, $\tilde{z}_0=0.118$, and $\langle H_{by}\rangle=-0.0437\chi H_{\text{ext}}$. This value is a factor of 1.9 times that for $\tilde{z}_0=0.36$ found above.

To illustrate the influence of the sensor aspect ratio, we consider a rectangular sensor with $\ell=3$. Using $2R=2$ μm and $t=100$ nm as above and requiring that $N_\ell=100$, we now find $w=10.7$ μm, $\tilde{z}_0=0.206$ and $\langle H_{by}\rangle=-0.0526\chi H_{\text{ext}}$. Thus, in this case, a further 17% increase of the average magnetic field can be obtained by using a rectangular sensor. It should be noted, however, that if ℓ is increased further, w becomes comparable to the bead diameter, and the continuous description of the bead distribution will only be valid for a statistical average of a number of sensors.

If a shielding layer is used to minimize the average magnetic field from beads outside the active area, it is likely that beads may tend to adhere near the edge and then a higher sensitivity to beads near the edge will be disadvantageous. In this case it may be better to choose values of R and t that minimize the edge effects. Thus, to maintain a minimum number of beads $\sim$100, a spacer layer should be introduced as discussed above. Although this spacer layer reduces the sensitivity of the sensor to the field from magnetic beads, it may in fact improve the sensitivity when used as a biosensor due to a reduced background from unspecifically bound beads near the sensor edge.

On the other hand, if the sensor can be functionalized on only the active area, and the unspecific binding of beads outside the sensor is minimal, it will be advantageous to use the thinnest possible spacer layer and choose a bead diameter and sensor size that maximize the average magnetic field according to the above guidelines. In our example above for a square sensor, we found that this resulted in a 90% increase of the average field relative to the case where $\tilde{z}_0=0.36$.

V. CONCLUSIONS

We have presented the first systematic study of the average in-plane magnetic field acting on square and rectangular sensors from magnetic beads as a function of the sensor dimension w, the spacer layer thickness t, a shielding layer thickness T, the bead susceptibility χ, and the bead diameter $2R$. General expressions for the sensor response were derived in terms of normalized variables such that the results can easily be adapted to a given application. We have considered both the response due to a single bead and due to a homogeneous distribution of magnetic beads in a single layer.

We have shown that the average magnetic field can be highly sensitive to the position of the bead on the sensor and for $2(R+t)/w\lesssim 0.3$ show negative peaks for beads inside the sensor area and positive peaks for beads outside the sensor area. We found that in most cases, it is not justified to assume that the sensor response is directly proportional to the number of beads. We have shown that the sensitivity to the position of beads placed on the sensor is minimal when the bead diameter is $2R=0.36w-2t$.

The average magnetic field from the beads and the number of beads that can fit onto a sensor has been systematically studied and discussed as a function of the sensor dimension and the thickness of the spacer layer.

We have presented two approaches on how to minimize the positive contributions, and their consequences for the sensor and bead parameters have been discussed. The first approach assumes a highly specific and localized bioassay that ensures that beads are only bound to the active sensor area. The second approach does not assume a localized functionalization in the bioassay but uses instead a shielding layer to minimize the average magnetic field from beads

placed outside the sensor area. The two different approaches were illustrated with numerical examples.

For both approaches, the largest sensor signal from a bead monolayer is obtained when the spacer layer thickness t is small compared to the sensor size and the bead diameter is comparable to the sensor size. Nevertheless, we argue that the sensor and bead dimensions should not only be chosen to maximize the sensitivity to the presence of magnetic beads but also to ensure a statistical averaging, which is sufficient for assessing the inevitable background of unspecifically bound magnetic beads.

For a sensor required to have space for a given number of beads, we have presented detailed guidelines for finding the optimum sensor dimension, bead diameter and spacer layer thickness, and for calculating the average magnetic field from a monolayer of beads on the active area. The use of the guidelines was exemplified for a square sensor with $t=100$ nm required to have space for 100 beads with parameters chosen to achieve minimum position dependency ($\tilde{z}_0 \approx 0.36$) and maximum response ($\tilde{z}_0$ minimized), respectively. For example, the average magnetic field in the maximum response case was found to be 90% higher than that in the minimum position dependency case.

ACKNOWLEDGMENTS

Financial support from the EU 6th Framework Programme BIODIAGNOSTICS project (Contract No. 017002) is greatly acknowledged by the authors.

[1] P. P. Freitas, H. A. Ferreira, D. L. Graham, L. A. Clarke, M. D. Amaral, V. Martins, L. Fonseca, and J. S. Cabral, in *Magnetoelectronics: Magnetoresistive Biochips*, edited by M. Johnson (Elsevier, Amsterdam, 2004).
[2] D. L. Graham, H. A. Ferreira, and P. Freitas, Trends Biotechnol. **22**, 455 (2004).
[3] P. Freitas, R. Ferreira, S. Cardoso, and F. Cardoso, J. Phys.: Condens. Matter **19**, 165221 (2007).
[4] M. Megens and M. Prins, J. Magn. Magn. Mater. **293**, 702 (2005).
[5] R. L. Edelstein, C. R. Tamanaha, P. E. Sheehan, M. M. Miller, D. R. Baselt, L. J. Whitman, and R. J. Colton, Biosens. Bioelectron. **14**, 805 (2000).
[6] J. C. Rife, M. M. Miller, P. E. Sheehan, C. R. Tamanaha, M. Tondra, and L. J. Whitman, Sens. Actuators, A **107**, 209 (2003).
[7] D. K. Wood, K. K. Ni, D. R. Schmidt, and A. N. Cleland, Sens. Actuators, A **120**, 1 (2005).
[8] G. Li, V. Joshi, R. L. White, S. X. Wang, J. T. Kemp, C. Webb, R. W. Davies, and S. Sun, J. Appl. Phys. **93**, 7557 (2003).
[9] G. Li, S. X. Wang, and S. Sun, IEEE Trans. Magn. **40**, 3000 (2004).
[10] G. Li, S. Sun, and S. X. Wang, J. Appl. Phys. **99**, 08P107 (2006).
[11] Y. Liu, W. Jin, Y. Yang, and Z. Wang, J. Appl. Phys. **99**, 08G102 (2006).
[12] R. Wirix-Speetjens, W. Fyen, J. De Boeck, and G. Borghs, J. Appl. Phys. **99** 103903 (2006).
[13] F. Cardoso, R. Ferreira, S. Cardoso, J. Conde, V. Chu, P. Freitas, J. Germano, T. Almeida, L. Sousa, and M. Piedade, IEEE Trans. Magn. **43**, 2403 (2007).
[14] P.-A. Besse, G. Boero, M. Demierre, V. Pott, and R. Popovic, Appl. Phys. Lett. **80**, 4199 (2002).
[15] L. Ejsing, M. F. Hansen, A. K. Menon, H. A. Ferreira, D. L. Graham, and P. P. Freitas, Appl. Phys. Lett. **84**, 4729 (2004).
[16] L. Ejsing, M. F. Hansen, A. K. Menon, H. A. Ferreira, D. L. Graham, and P. P. Freitas, J. Magn. Magn. Mater. **293**, 677 (2005).
[17] H. A. Ferreira, N. Feliciano, D. L. Graham, and P. P. Freitas, J. Appl. Phys. **97**, 10Q904 (2005).